search for replacement and alternative agents. The superior attributes of halon 1301 have not yet been matched by agents with acceptable levels of toxicity, ozone-depletion potential, and global warming potential. As halon 1301 is replaced with a possibly less effective agent, improvements to fire-suppression systems have become important to enhance their performance and efficient use of the agent. Fires in aircraft engine nacelles, dry bays, shipboard machinery space, or ground armored vehicle compartments often occur in a complex geometry under highly ventilated conditions. A recirculation zone behind clutter such as flanges, pipes, or steps provides conditions favorable for flame holding (Raghunandan and Yogesh, 1989; Rohmat et al., 1998), i.e., lower velocities, heat recycling to the flame stabilizing region; augmented heat transfer to condensed fuel surfaces; and enhanced mixing of fuel, air, and hot combustion products. In addition, the complex geometry also affects the dynamics of an agent entrained in the fire zone. Therefore, fluid mechanics and flame stability behind an obstruction may be a dominant factor affecting the performance of fire-suppression agents (Moussa, 1994).

Few results have been reported in the literature on the suppression of obstruction-stabilized nonpremixed flames. Hirst and Sutton (1961), Hirst et al (1976, 1977), and Dyer et al. (1977a, 1977b) studied baffle-stabilized kerosene pool fires in a wind tunnel and concluded that the most stable type of flame to be encountered in an aircraft engine fire is a liquid surface diffusion flame from a pool of fuel burning behind an obstruction in an airflow. For the suppression of baffle-stabilized JP-8 spray flames, Hamins et al. (1996) identified two crucial parameters; i.e., a characteristic mixing time in the recirculation zone and the critical agent concentration at suppression for long agent injection durations and derived a theoretical expression for the critical agent mole fraction as a function of the injection duration. In a previous paper (Takahashi et al., 2000), the authors reported for the first time the results of characteristic mixing time measurements using obstruction-stabilized methane flames and incorporated the results into the correlation between the critical mole fraction at suppression and the agent injection period.

The role of computational modeling and simulations of fire dynamics and suppression has gained importance in recent years as a result of progress in understanding of the subject phenomena and the rapid growth of computational capabilities. The fire and suppression models for cluttered compartments are currently under development (Gritzo et al., 1999; Tieszen and Lopez, 1999) with particular emphasis on the applications to fires in aircraft dry bays, fuel tanks, engine nacelles, ground vehicle crew and engine compartments, shipboard machinery, and occupied spaces, etc. Computational models must be validated and/or calibrated by experimental data to develop practical, credible engineering



tools for the design of efficient fire protection systems using the best available agents.

The objectives of this study are to gain a better understanding of the flame stabilization and suppression behavior of obstacle-stabilized nonpremixed flames and to obtain experimental data to set coefficients in fire-suppression submodels. The fire-suppression submodels will then be tested (Gritzo et al., 1999; Tieszen and Lopez, 1999) in a spectrum of applications to ensure applicability outside the narrow range of experimental data. In addition to the baseline suppression-limit data previously obtained (Takahashi et al., 2000) for step-stabilized methane flames using halon 1301, new results are reported in this paper using various types of fuels, fire-extinguishing agents, and obstructions. Furthermore, planar laser-induced fluorescence (PLIF) of hydroxyl (OH) radicals was used to characterize the spatial burning variations in the recirculation zone. An attempt is made to obtain a universal suppression-limit curve valid for various parameters and to extract physical insights into underlying mechanisms common in obstacle-stabilized flames.

## EXPERIMENTAL TECHNIQUES

### Experimental Apparatus

The fire-suppression test facility, described elsewhere (Takahashi et al., 2000), has been modified to accommodate specific requirements for a large volume of an inert-gas agent (nitrogen) and a liquid fuel (JP-8). Figure 1 shows the experimental apparatus, which consists of the fuel, air, and agent supply systems, a horizontal small-scale combustion tunnel (154-mm square cross-section, 77-cm length) with quartz windows. A water-cooled porous plate (150-mm square × 12.7-mm thickness, 316L stainless steel) is placed flush with the bottom surface of the test section downstream of an obstruction. The flow rate of a gaseous fuel (methane or ethane) is arbitrary set at 10 l/min (heat release: 5.45 kW and 9.73 kW for methane and ethane, respectively), which results in a low mean (upward) fuel velocity (0.7 cm/s) typical of pool flames. The obstructions used (see Fig. 1 inset), described in detail elsewhere (Takahashi et al., 2000), are a right-angle backward-facing step (height, $h_s$= 32 mm or 64 mm), a 45°-angle backward-facing step ($h_s$ = 64 mm), and an inverted-J-shape flange ($h_s$ = 64 mm; downstream overhang: 38-mm length × 13-mm height with 6-mm-radius corners). The angled step is used in consideration of a helical flow induced by the circumferential agent injection in the annular aircraft engine nacelle. The J-flange mimics mechanical strengthening members in the engine bay.

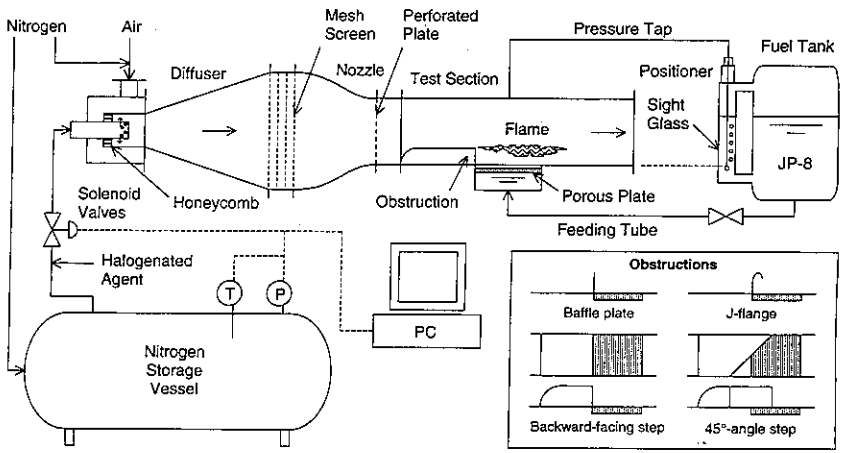


FIGURE 1 The experimental apparatus

For JP-8, the water-cooled porous plate is lowered about 6.4 mm from the bottom surface to form a shallow liquid-fuel pool over the plate. A liquid fuel supply and leveling system consists of a sealed fuel tank (volume: 7.6 l), a liquid fuel feeding tube connecting the bottom of the fuel tank and the porous plate housing, and a pressure tap tubing extending from the top of the test section to the other open end emerging into the fuel tank sight glass. By adjusting the height of the tip of the pressure tap tubing in the sight glass using a micro-positioner, the liquid level in the test section can be finely adjusted.

The airflow is conditioned by passing through honeycombs, a diffuser, mesh screens (#100), a contoured contraction nozzle, and a turbulence-generating perforated plate (33% opening, 2.4-mm-dia. holes), which generates turbulence levels up to ~6%. The mean air velocities at the test section inlet ($U_{a0}$) and the obstruction ($U_{as}$) are calculated by dividing the volumetric air flow rate ($Q_a$) by the cross-sectional areas of the full test section and the air passage above the obstruction, respectively. Hence, $U_{as} = [1/(1\text{-}h_s/h_T)]U_{a0}$, where $h_T$ (0.154 m) is the total height of the test section. The effective mean air velocity is then calculated as $U_a^* = (U_{a0} + U_{as})/2$.

The transient agent supply system (Takahashi et al., 2000) for halogenated suppressants, which is similar in principle to that of Hamins et al. (1994a, 1995, 1996), has been used for halon 1301 or HFC-125 (pentafluoroethane, $C_2HF_5$) to extinguish JP-8 pool flames and modified for nitrogen, which requires an order-of-magnitude greater concentration to extinguish flames than halogenated



suppressants. For nitrogen, two sets of agent storage vessels and computer-controlled parallel solenoid valves are used, depending on the air flow condition: (1) for $U_{a0} = 7.1$ m/s, two connected vessels (2 × ~300 l or ~300 l + ~600 l) and up to eight valves (Peter Paul 72T10DCM, response time: ~12 ms); (2) for $U_{a0} = 10.8$ m/s, a large vessel (~3700 l) and eight valves (ASCO 8210G3).

The gaseous agent was injected impulsively into the airflow ~1 m upstream of the flame. Uniform agent dispersion into the airstream was achieved by injecting the agent perpendicular to the airflow in a reduced diameter (108 mm) section through up to 32 × 6.4-mm-dia. holes in four rows in a 25.4-mm-o.d. closed-end tube for $U_{a0} = 7.1$ m/s, or 30 × 9.5-mm-dia. holes in four rows in a 50.8-mm-o.d. closed-end tube for $U_{a0} = 10.8$ m/s. The mesh screens and a perforated plate downstream enhance further mixing. The schlieren visualization performed previously (Takahashi et al., 2000) for halon 1301 revealed fairly good agent dispersion and mixing in air. The agent temperature and pressure in the storage vessel are measured with a T-type (copper-constantan) thermocouple and a pressure transducer (Druck PTX-620). The amount of injected agent is controlled by varying the initial storage vessel pressure and the time period that the valve is open and is determined from the difference between the initial and final pressures and temperatures in the storage vessel using the ideal-gas equation of state. Because the sufficiently large storage volume results in a relatively small pressure drop during agent discharge and the valve response time is relatively short compared to the agent injection period, a constant agent discharge rate is assumed. Therefore, the mean volumetric agent concentration is determined by dividing the mean agent flow rate ([volume]/[injection period]) by the total (air and agent) flow rate.

The continuous nitrogen supply system for steady-state fire suppression experiments consists of high-pressure (up to 170 atmg) nitrogen vessels on a trailer, dome pressure regulators, a rupture disk, a calibrated critical flow nozzle (Flow-Dyne, throat dia.: 4.90 mm), a pressure transducer, and a T-type thermocouple. The mass flow rate of nitrogen is determined from the measured pressure and temperature upstream of the critical flow nozzle.

## Flame Suppression Limit Measurements

The transient fire suppression limit experiment is conducted as follows. First, a stable flame is established for a fixed air velocity for a period of at least 20 min, and the agent is injected for a particular storage vessel pressure and injection period to determine whether or not the flame extinguishes. When extinguished, the flame is re-ignited using a propane-torch-assisted spark igniter equipped on the back wall of the test section. The agent injection test is repeated 20 or 50

times for halogenated agents or nitrogen, respectively, and the probability of suppression is determined by dividing the number of extinguishments by the total number of runs. Then either the storage vessel pressure (which determines agent concentration) or injection period is varied step-wise and the experiment is repeated. The suppression condition is confirmed at a probability of 90% chosen arbitrarily. The steady-state fire suppression limit experiment is conducted by gradually adding nitrogen into the air by maintaining the air flow rate constant until the flame extinguishes. The maximum relative error of the flame suppression limit was estimated as ±8% for pool flames with halogenated agents and ±4% and ±2% for gaseous flames with nitrogen for transient and steady-state measurements, respectively.

### Planar Laser-induced Fluorescence Measurements

OH PLIF images are acquired to characterize the spatial burning variations without agent injection using a right-angle or 45°-angle backward-facing step at a mean inlet air velocity of 7.1 m/s. The OH PLIF system (Fig. 2), which is similar to that used by Donbar et al. (2000), consists of a pulsed Nd:YAG laser (Quanta Ray DCR-24–10), a dye laser (Spectra Physics PDL-2), a doubling crystal (Inrad Auto Tracker II), a harmonic separator (Inrad 752–104), and an intensified charge-coupled device camera (Princeton Instruments ICCD-576S/B, 576 × 384 pixels). OH fluorescence is obtained by tuning a Nd:YAG-pumped dye laser to the $R_1(8.5)$ transition of the $A^2\Sigma^+$-$X^2\Pi$ ($v' = 1$, $v'' = 0$) band ($\lambda = 281.34$ nm) and fluorescence from the A-X (1,1) and (0,0) bands ($\lambda = 306$–$320$ nm) is collected with a lens (UV Nikkor 105 mm/f4.5) and imaged onto a PI ICCD array. To improve the signal-to-noise ratio, each 2-by-2 pixel region is spatially averaged; thus the spatial resolution of each OH image is the area that is imaged on two pixels, or 0.65 mm.

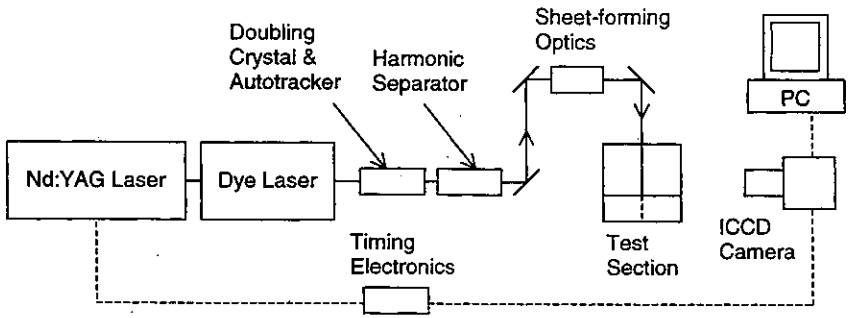


FIGURE 2 The OH Planar laser-induced fluorescence system



## RESULTS AND DISCUSSION

### Optical Observations

Figure 3 shows direct and schlieren photographs of methane flames stabilized behind a right-angle backward-facing step. In the previous paper (Takahashi et al., 2000), we reported two distinct flame stabilization and suppression regimes; i.e., (I) rim-attached and (II) wake-stabilized, depending on the mean air velocity. In regime I (Fig. 3a, $U_{a0} = 1.4$ m/s), a luminous (sooty), continuously wrinkled laminar flame zone was formed as a result of interactions of the diffusion flame zone and large-scale vortices evolved and developed in the free shear layer. In regime II (Fig. 3b, $U_{a0} = 7.1$ m/s), the flame zone in the shear layer detached and became a turbulent blue flame. Separate blue flame zones with sporadic yellow flashes were formed in the recirculation zone as a result of dynamic air entrainment. The regime-II flames are more likely to occur in highly ventilated fires.

Figure 3c shows the instantaneous schlieren photograph (partial view) of a regime-II flame ($U_{a0} = 7.1$ m/s) at the event of suppression by halon 1301. The agent was released into the airflow for duration of 0.25 s. Because the knife-edge of the schlieren system was placed vertical, the image showed the horizontal gradient of the refractive index field, which depended primarily on the density and, thus, the reciprocal of the temperature. In addition, the schlieren deflectometry was able to capture the wave of agent-laden airflow as a fine irregularity due to the agent's high molecular weight (149). In regime II, a detached turbulent flame was formed in the shear layer, where the small-scale turbulence coexisted with the large-scale vortices, and flame elements were also visualized as oblique dark zones in the recirculation zone. In Fig. 3c, the agent just arrived (at 0.145 s after injection) and the shear layer flame was already affected. Unfortunately, the location of the flame zone is somewhat ambiguous because schlieren imaging is a line-of-sight technique and the flame is not completely two-dimensional due to the three-dimensional nature of turbulent motions.

Figure 4 shows OH PLIF images of methane flames stabilized behind a right-angle backward-facing step, revealing spatial burning variations and the dynamic features of the flame zone in the shear layer and the recirculation zone in the wake of the step. In general, the OH radicals were contained in relatively narrow zones, indicative of wrinkled sheet-like diffusion flames. The broadened lower-intensity regions on lower left (fuel) side of the bright OH zones are thought to be scattering from soot particles (or polycyclic nuclear aromatic hydrocarbons) in fuel pyrolysis zones, which were observed as yellow flashes by the naked eye. Figure 4a shows the flame zone, which was stabilized (but not attached) by the step edges and developed in the shear layer. The flame was

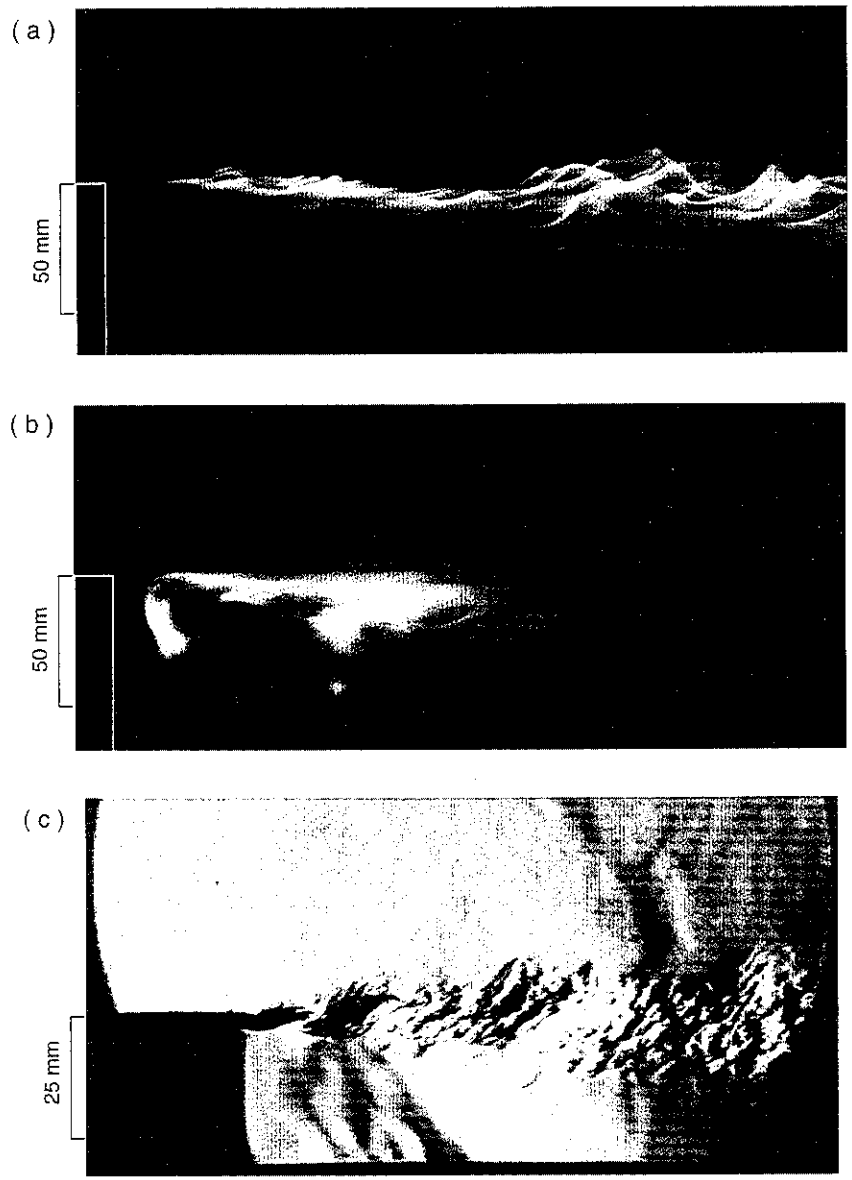


FIGURE 3 Photographs of methane flames stabilized behind a right-angle backward-facing step. Film: KODAK EPH-1600. (a) Direct time exposure (f5.6, 1/4000 s), $h_s = 64$ mm, $U_{a0} = 1.4$ m/s (Regime I); (b) direct time exposure (f1.4, 1/125 s), $h_s = 64$ mm, $U_{a0} = 7.1$ m/s (Regime II); (c) instantaneous (~1 μs) schlieren, $h_s = 32$ mm, $U_{a0} = 7.1$ m/s (Regime II) (See Color Plate III at the back of this issue)



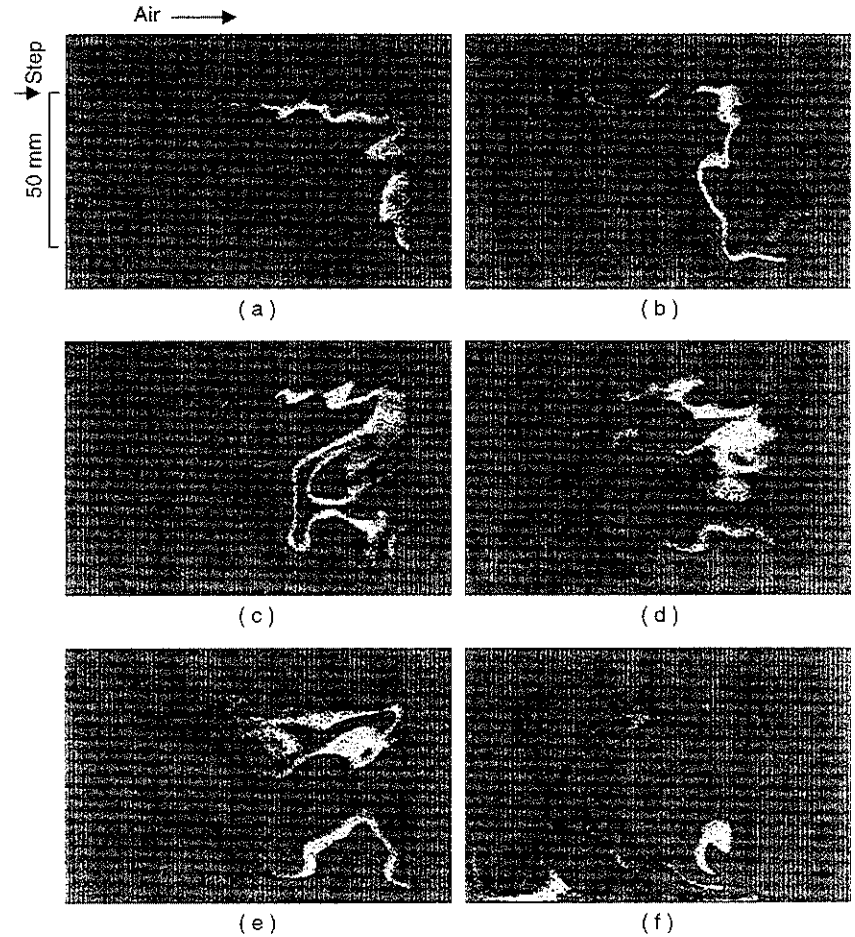


FIGURE 4 Instantaneous (10 ns) OH planar laser-induced fluorescence images of methane flames stabilized behind a right-angle backward-facing step. $h_s$= 64 mm, $U_{a0} = 7.1$ m/s (Regime II) (See Color Plate IV at the back of this issue)

wrinkled as a result of interactions with large-scale vortices evolved and developed in the shear layer. The local extinction, or separation, of the shear layer flame was obvious in Figs. 4b through 4d. Unlike visual observations of the flame by the naked eye, the behavior of the flame zone represented by the OH zones was totally dynamic. Although the images in Fig. 4 are not in an actual time sequence, general features of the dynamic behavior of the flame can be extracted. As a result of a back flow of air entrained into the recirculation zone,

the shear layer flame was folded along the fuel-air interface and penetrated deeply into the recirculation zone (Figs. 4a through 4e). A mushroom shaped vortex is evident in Fig. 4c. As the packet of fuel burning in the shear layer (the upper side in Fig. 4e) was consumed, only the flame in the recirculation zone remained momentarily (Fig. 4f). As the fresh fuel emerged and ignited behind the flame in the recirculation zone, a shear layer flame might redevelop (Fig. 4a) and repeat the oscillatory process.

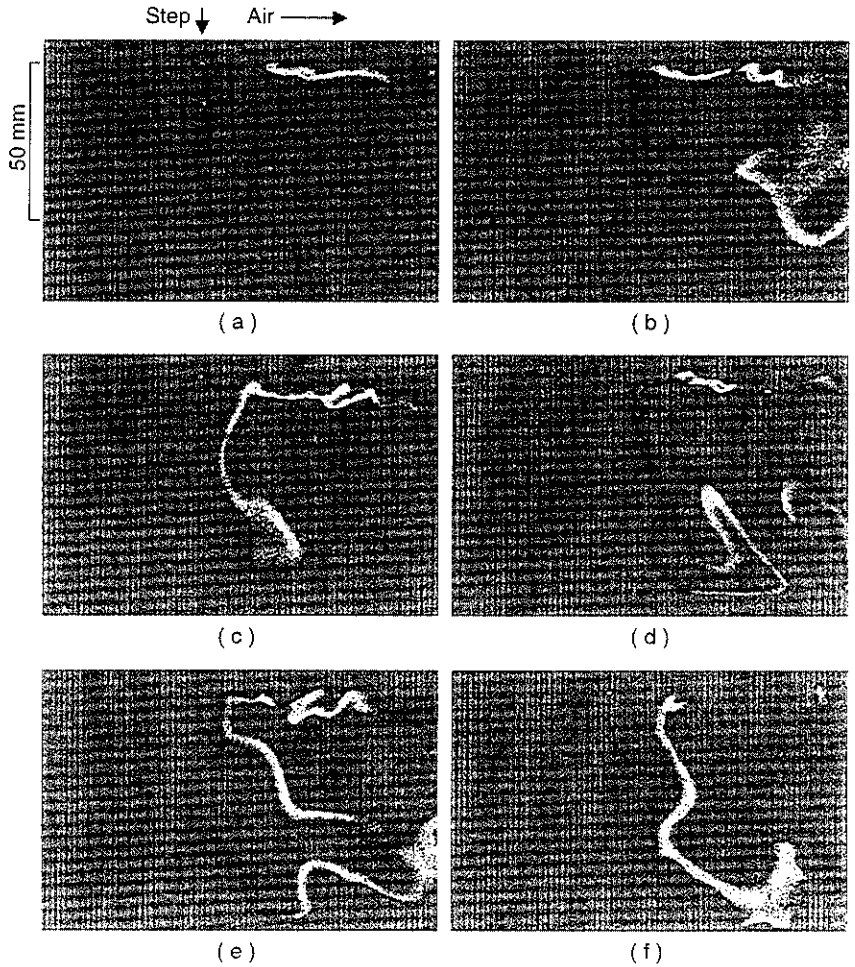


FIGURE 5 Instantaneous (10 ns) OH planar laser-induced fluorescence images of methane flames stabilized behind a 45°-angle backward-facing step. $h_s = 64$ mm, $U_{a0} = 7.1$ m/s (Regime II) (See Color Plate V at the back of this issue)



OH PLIF images in Fig. 5 revealed a feature peculiar to a 45°-angle step. Figures 5a and 5b show the shear layer flame and the flame folding phenomena described above. In addition to the dynamic behavior due to the back flow of the entrained air, the flame zone extended downward near the step (Figs. 5c through 5e) probably because air penetrated along the step wall toward the inside corner, where a counter-rotating recirculation zone was formed. As the local extinction of the shear layer flame spread, the flame near the wall remained (Fig. 5f). Although it is beyond the scope of this paper, the three-dimensional flow field measurement is needed to further investigate the peculiar flame dynamics.

## Suppression Limits for Long Agent Injection Periods

The critical agent mole fractions in the oxidizer stream at suppression ($X_c$) were measured by the transient method at various agent injection periods ($\Delta t$) and the steady-state method. Figure 6 shows the probability of extinction ($P_{ext}$) of ethane flames as a function of the mole fraction of injected nitrogen in the oxidizer stream ($X_{N_2}$) for a sufficiently long injection period ($\Delta t = 2$ s) and $U_{a0} = 7.1$ m/s (regime II). Thus, for the transient method, the critical agent (nitrogen) mole fraction at suppression for long injection periods ($X_\infty$) was determined at $P_{ext} = 0.9$ as 0.365 for ethane and, in the same manner, as 0.292 for methane. For the JP-8 pool flames, $X_\infty$was 0.04 and 0.087 for halon 1301 and HFC-125, respectively, for $\Delta t = 1$ s or 2 s and $U_{a0} = 7.1$ m/s. These $X_\infty$values indicate that HFC-125 requires a volume factor of ~2, compared to halon 1301, as is consistent with the previous result (Hamins et al., 1994a).

By using the steady-state method, the critical nitrogen mole fraction at suppression of ethane flames was determined at $U_{a0} = 10.9$ m/s as 0.347, which corresponded to a value for the transient method of $P_{ext} = 0.5$ (Fig. 6). At higher nitrogen concentrations, the flame could not be sustained continuously even with repeated re-ignition by the igniter. It is reasonable that for the steady-state measurement, the flame suppression occurred at a nitrogen mole fraction less than the critical value at the transient suppression probability of $P_{ext} = 0.9$.

Although one would anticipate that the flame would blow out by increasing the airflow velocity with no agent added, baffle-stabilized flames are very stable. Hirst and Sutton (1961) showed that the extinction velocities of baffle-stabilized kerosene flames increased monotonically with increasing pressure (0.1–0.8 atm) and height of projection up to an optimum size of plate (~16 mm) and then decreased. The extinction velocity at 1 atm, extrapolated from their data for the plate height of 51 mm, would be over 40 m/s. Therefore, the present experimental conditions ($U_{a0} < 10.9$ m/s) must be substantially less than the extinction limit

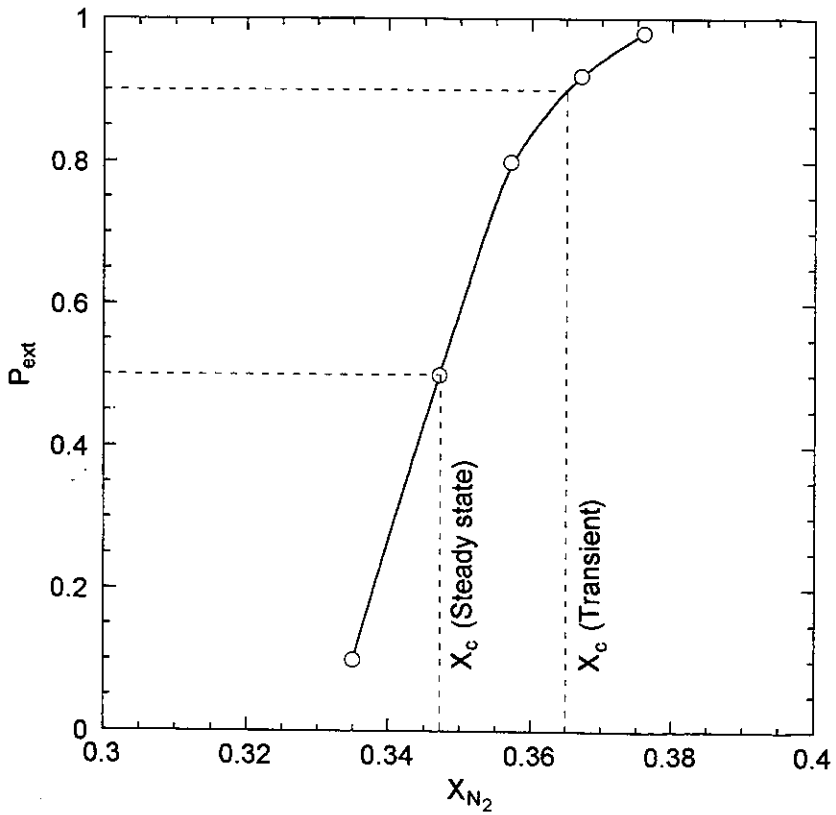


FIGURE 6 The probability of extinction of ethane flames as a function of the mole fraction of injected nitrogen in the oxidizer stream for a long injection period ($\Delta t = 2$ s). $h_s = 64$ mm, $U_{a0} = 7.1$ m/s (Regime II)

without agent, and thus, $X_\infty$ measured here appears to be independent of the air velocity within the experimental range.

Table I compares the suppression limits for the present obstruction-stabilized flames with the extinction limit data in the literature obtained for various fuels by cup burners (Hirst and Booth, 1977; Bajpai, 1974; Sheinson et al., 1989; NFPA, 1994; Hamins et al., 1994a; Sakai et al, 1995; Saito et al., 1996; Moor et al., 1996; Babb et al., 1999), counterflow diffusion flames (Simmons and Wolfhard, 1957; Tsuji, 1982; Hamins et al., 1994b; Saso et al., 1996; Papas et al., 1996; Pitts and Blevins, 1999) turbulent spray flames (Hamins et al, 1994a, 1996), and baffle-stabilized pool fire (Dyer et al., 1977a). The former two are the



steady-state methods and the latter two are the transient methods, for which the $X_c$ values for long injection periods ($X_\infty$) are listed. Hence, Simmons and Wolfhard (1957) and Tsuji (1982) determined the limiting oxygen index ($\chi_{O_2}$) using hemispherical and cylindrical counterflow diffusion flames, respectively. The limiting oxygen index is the mole fraction of oxygen in the oxidizer stream below which no flame can be stabilized irrespective of the stagnation velocity gradient (i.e., strain rate). Thus, Table I includes both the critical agent mole fractions and the limiting oxygen indices in the oxidizer stream at suppression. The conversion between the two quantities can be made using the relationship:

$$\chi_{o_2} = 0.2093(1 - X_c) \tag{1}$$

Although $\chi_{O_2}$ has been used for inert-gas agents, $X_c$ is more distinguishable for halogenated agents, for which $X_c$ is much smaller than unity and thus $\chi_{O_2}$ does not vary much.

For nitrogen as the agent, the $X_c$ values for counterflow diffusion flames (0.32 – 0.336 for methane, 0.436 for ethane, 0.393 for propane), particularly by Simmons and Wolfhard (1957), were higher than those for present wake-stabilized (regime II) turbulent flames (0.292 for methane, 0.347 – 0.365 for ethane) and cup-burner flames (0.325 for propane). $X_c$'s for heptane flames using cup burners by various investigators (0.30 – 0.336) were scattered around a value for relatively low strain-rate flat counterflow flames (0.31 for $a = 50$ s$^{-1}$). The $X_c$ values using hemispherical counterflow flames by Simmons and Wolfhard (1957) (0.362 for hexane, 0.36 for octane, and 0.357 for decane) were nearly the same and identical to that for a flat counterflow heptane flame at the lowest strain rate listed (0.36 for $a = 24$ s$^{-1}$). As expected, the $X_c$ value for the couterflow flame at a high strain rate (360 s$^{-1}$) was low (0.118). Interestingly, the baffle-stabilized kerosene pool fire resulted in the highest $X_c$ value (0.38) among all fuels listed.

As reported in the previous paper (Takahashi et al., 2000), the critical agent mole fraction at suppression at long injection periods for rim-attached (regime I) and wake-stabilized (regime II) methane flames extinguished with halon 1301 was the same (0.025) and identical to that obtained in the counterflow diffusion flame (Papas et al., 1996). The critical agent mole fraction for step-stabilized JP-8 pool flames with halon 1301 (0.04) was higher than $X_c$'s for JP-8 and heptane using cup burners (0.029 – 0.035) and counterflow flames (0.027 – 0.031) at relatively low strain rates (30 – 45 s$^{-1}$). The present result for step-stabilized JP-8 pool flames with HFC-125 (0.087) was identical to that for cup burners and among the scatter of the data (0.081 – 0.094) for both JP-8 and heptane using cup burners and counterflow flames. The value for turbulent spray flames (0.078), which might have lower flame stability, was slightly lower than the others. In

summary, a general trend in $X_c$'s for various burner systems, flow conditions, and researchers, in a descending order is as follows:

$$\text{Hemispherical counterflow (cf)} \approx \text{flat cf } (a = 24\ \text{s}^{-1}) > \text{step-stabilized}$$
$$\approx \text{cup burner} \approx \text{flat cf } (a = 30 - 50\ \text{s}^{-1})$$
$$\approx \text{turbulent spray} > \text{flat cf } (a = 360\ \text{s}^{-1})$$

Here, $X_c$'s for step-stabilized flames might have a wide spread from the lowest (methane/nitrogen) to the highest (kerosene/nitrogen and JP-8/halon 1301) among each group probably because there were many uncontrolled variables affecting the extinction phenomena. Nevertheless, $X_c$'s for the step-stabilized flames did not deviate much from the scattered data range for various burner systems with vastly different flow conditions. This result suggested that the suppression mechanism was essentially the same, except for the counterflow flames at high strain rates ($a \sim 360\ \text{s}^{-1}$), which were extinguished primarily by aerodynamic stretch.

## Suppression Limit Dependency on Agent Injection Period

Figure 7 shows the critical agent mole fraction at suppression as a function of the agent injection period at different mean initial air velocities for methane, ethane (Fig. 7a), and JP-8 flames (Fig. 7b). In Fig. 7a, the critical agent (nitrogen) mole fractions remained constant at the $X_\infty$ values (0.292 and 0.365 for methane and ethane, respectively) in the range of 0.5 s < $\Delta t$ < 2 s and increased as $\Delta t$ was decreased further. The experiment for short agent injection periods was limited by the volume of nitrogen storage vessel and the solenoid valve response time. Thus, minimum injection periods, below which the flame could not be extinguished even at high agent concentrations, could not be determined, unlike the case for methane with halon 1301 reported previously (Takahashi et al., 2000).

For the JP-8 pool flames (Fig. 7b), the dependencies of the critical agent mole fraction on the injection period were determined for various experimental parameters: the agent type, obstruction shape, height, and the mean air velocity. The general trends were the same as the previous results (Takahashi et al., 2000) for methane flames extinguished with halon 1301; the critical agent mole fraction at suppression increased as the injection period was decreased. Any parameter variation, which increases the characteristic mixing time, i.e., increased obstruction height or decreased air velocity, also increased $X_c$. For halon 1301, the theoretical suppression-limit curve (to be described later) for $\tau = 0.5$ s was just about passing the condition for the design criterion for the current halon fire-extinguishing system in the aircraft engine nacelle; i.e., a minimum agent concentration (about 6% by volume) must be maintained throughout the nacelle for a



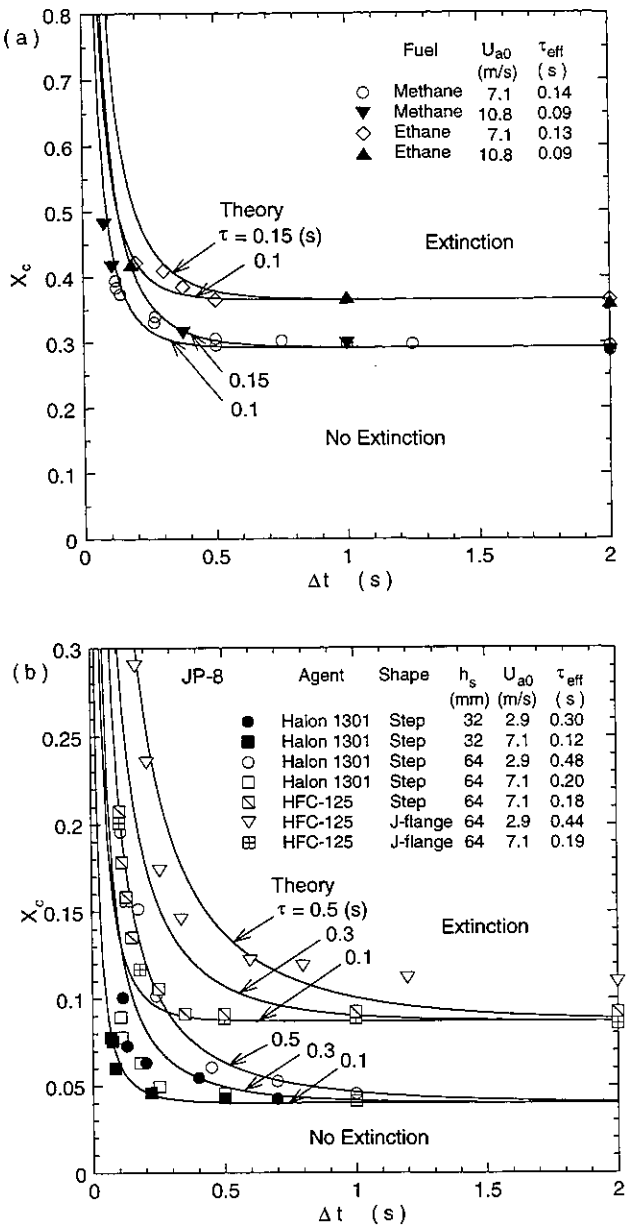


FIGURE 7 Measured critical agent mole fraction in the oxidizer stream at suppression and theoretical curves as a function of the agent injection period. (a) Agent: nitrogen; fuel: methane and ethane. Obstruction: right-angle backward-facing-step ($h_s$ = 64 mm). (b) Agent: halon 1301, HFC-125; fuel: JP-8

minimum time interval (about 0.5 s) to ensure that the fire will be extinguished and not re-light. Thus, the obstruction-stabilized fires, in which the characteristic mixing time is greater than ~0.5 s (the upper-right side of the curve), may not be extinguished by a system whose performance does not exceed the current design criterion. Therefore, the physical time is inappropriate to be used for the design criterion because the suppression limits depend also on the characteristic mixing time, a function of the obstruction size and the flow velocity.

For HFC-125, no difference in the suppression limits for the step and J-flange were found at $U_{a0} = 7.1$ m/s, and the $X_\infty$value (0.087) was maintained in the range of 0.3 s < $\Delta t$ < 2 s. At a lower air velocity ($U_{a0} = 2.9$ m/s, regime I → II transitional), $X_c$ for HFC-125 decreased to 0.1 at $\Delta t = 2$ s but did not approach the minimum value. The similar trend of a higher minimum agent (HFC-125) mole fraction at a low air velocity was also observed by Hamins et al. (1996) for an axisymmetric baffle-stabilized JP-8 spray flame (0.078 and 0.10 at the air velocities of 7.5 m/s and 3.0 m/s, respectively). The critical agent mole fraction may further decrease for much longer injection periods, as was observed previously (Fig. 9c in Takahashi et al., 2000) for methane flames with halon 1301.

Theoretical curves in Fig. 7 were derived by Hamins et al. (1996) based on a phenomenological model for a well-stirred reactor developed by Longwell et al. (1953):

$$X_c = \frac{X_\infty}{1 - e^{(-\Delta t/\tau)}} \tag{2}$$

Hence, $\tau$ is the characteristic mixing time for entrainment into the recirculation zone. The measured values of $X_\infty$ were used in the plot. For a long injection period, Eq. 2 becomes $X_c \approx X_\infty$, i.e., a minimum value ($X_\infty$) is sufficient for the free stream mole fraction ($X_c$) to achieve $X_\infty$ in the recirculation zone to extinguish the flame. Thus, $X_\infty$ is theoretically the same as the steady-state conditions as listed in Table I. For a short injection period, large free stream agent mole fractions ($X_c > X_\infty$) were required to achieve the same condition in the recirculation zone within the available time.

The characteristic mixing time ($\tau_{exp}$) was measured previously (Takahashi et al., 2000) by the sodium emission method (Winterfeld, 1965) as the reciprocal of the rate constant for the exponential turbulent material exchange process between the recirculation zone and the free stream. A linear correlation (Takahashi et al., 2000) was obtained for various obstructions (right-angle and 45°-angle backward-facing steps, baffle plate, and J-flange) as:

$$\tau_{exp} = 34.7(h_s/U_a^*) \tag{3}$$



TABLE I Comparisons of the Extinction Limit Data

| *Agent* | *Fuel* | *Critical Agent Mole Fraction* $X_c$ | *Limiting Oxygen Index*[a] $\chi_{O_2}$ | *Flame Configuration*[b] | *Researcher* |
|---|---|---|---|---|---|
| Nitrogen | Methane | 0.292 | 0.148 | Step-stabilized flame, transient | This study |
| | Methane | 0.336 | 0.139 | Counterflow flame, hemispherical | Simmons & Wolfhard (1957) |
| | Methane | 0.32 | 0.143 | Counterflow flame, cylindrical | Tsuji (1982) |
| | Methane | 0.33 | 0.140 | Counterflow flame, estimate | Pitts & Blevins (1999) |
| | Ethane | 0.365 | 0.133 | Step-stabilized flame, transient | This study |
| | Ethane | 0.347 | 0.137 | Step-stabilized flame, steady-state | This study |
| | Ethane | 0.436 | 0.118 | Counterflow flame, hemispherical | Simmons & Wolfhard (1957) |
| | Propane | 0.393 | 0.127 | Counterflow flame, hemispherical | Simmons & Wolfhard (1957) |
| | Propane | 0.325 | 0.141 | Cup burner | Hamins et al. (1994a) |
| | Hexane | 0.362 | 0.1335 | Counterflow flame, hemispherical | Simmons & Wolfhard (1957) |
| | Heptane | 0.302 | 0.146 | Cup burner | Hirst & Booth (1977) |
| | Heptane | 0.30 | 0.147 | Cup burner | Sheinson et al. (1989) |
| | Heptane | 0.32 | 0.142 | Cup burner | Hamins et al. (1994a) |
| | Heptane | 0.30 | 0.147 | Cup burner | Moore et al. (1996) |
| | Heptane | 0.336 | 0.139 | Cup burner | Sakai et al. (1995), Saito et al. (1996) |
| | Heptane | 0.33 | 0.140 | Cup burner | Babb et al. (1999) |
| | Heptane | 0.31 | 0.144 | Counterflow flame, flat, $a = 50\ s^{-1}$ | Hamins et al. (1994a, 1994b) |
| | Heptane | 0.118 | 0.185 | Counterflow flame, flat, $a = 360\ s^{-1}$ | Hamins et al. (1994a, 1994b) |
| | Heptane | 0.36 | 0.134 | Counterflow flame, flat, $a = 24\ s^{-1}$ | Saso et al. (1996) |
| | Octane | 0.360 | 0.134 | Counterflow flame, hemispherical | Simmons & Wolfhard (1957) |
| | Decane | 0.357 | 0.1345 | Counterflow flame, hemispherical | Simmons & Wolfhard (1957) |
| | Kerosene | 0.38 | 0.130 | Baffle-stabilized pool fire | Dyer et al. (1977a) |

| *Agent* | *Fuel* | *Critical Agent Mole Fraction* $X_c$ | *Limiting Oxygen Index*[a] $\chi_{O_2}$ | *Flame Configuration*[b] | *Researcher* |
|---|---|---|---|---|---|
| Halon 1301 | Methane | 0.025 | 0.204 | Step-stabilized flame, transient | Takahashi et al. (2000) |
| | Methane | 0.025 | 0.204 | Counterflow flame, flat | Papas et al. (1996) |
| | JP-8 | 0.04 | 0.201 | Step-stabilized flame, transient | This study |
| | JP-8 | 0.031 | 0.203 | Cup burner | Hamins et al. (1994a) |
| | JP-8 | 0.027 | 0.204 | Counterflow flame, flat, $a = 45\ s^{-1}$ | Hamins et al. (1994a, 1994b) |
| | JP-8 | 0.033 | 0.202 | Turbulent spray flame | Hamins et al. (1994a, 1996) |
| | Heptane | 0.033 | 0.202 | Cup burner | Bajpai (1974) |
| | Heptane | 0.035 | 0.202 | Cup burner | Hirst & Booth (1977) |
| | Heptane | 0.031 | 0.203 | Cup burner | Sheinson et al. (1989) |
| | Heptane | 0.031 | 0.203 | Cup burner | Hamins et al. (1994a) |
| | Heptane | 0.029–0.035 | 0.202–0.203 | Cup burner | NFPA (1994) |
| | Heptane | 0.034 | 0.202 | Cup burner | Sakai et al. (1995), Saito et al. (1996) |
| | Heptane | 0.031 | 0.203 | Counterflow flame, flat, $a = 45\ s^{-1}$ | Hamins et al. (1994a, 1994b) |
| | Heptane | 0.03 | 0.203 | Counterflow flame, flat, $a = 30\ s^{-1}$ | Saso et al. (1996) |
| HFC-125 | JP-8 | 0.087 | 0.191 | Step-stabilized flame, transient | This study |
| | JP-8 | 0.087 | 0.191 | Cup burner | Hamins et al. (1994a) |
| | JP-8 | 0.083 | 0.192 | Counterflow flame, flat, $a = 50\ s^{-1}$ | Hamins et al. (1994a) |
| | JP-8 | 0.078 | 0.193 | Turbulent spray flame | Hamins et al. (1994a, 1996) |
| | Heptane | 0.081–0.094 | 0.190–0.192 | Cup burner | NFPA (1994) |
| | Heptane | 0.087 | 0.191 | Cup burner | Hamins et al. (1994a) |
| | Heptane | 0.085 | 0.192 | Counterflow flame, flat, $a = 45\ s^{-1}$ | Hamins et al. (1994a) |

a. Converted from the critical agent mole fraction except for the values by Simmons & Wolfhard (1957) and Tsuji (1982).
b. $a$ is the effective strain rate ($2V/L$; $V$: the injection velocity, $L$: the burner separation; Hamins et al., 1994b) for counterflow diffusion flames.



Because the definition of the characteristic mixing time is based on the time constant for the mathematical (exponential decay) function, it is reasonable to define further an effective mixing time for the specific physical phenomenon (suppression limit) as $\tau_{eff} = C\tau_{exp}$. The coefficient $C$ was determined by plotting the data points in $(1 - X_\infty/X_c)$ vs. $\exp[-\Delta t/(\tau_{eff})]$ with various $C$ values until the linear correlation gives a slope of unity (the equality of these variables). Figure 8 includes the previous data for methane flames extinguished with halon 1301 (Fig. 10 in Takahashi et al., 2000) as well as the present data (Fig. 7). In the previous paper (Takahashi et al., 2000), because of relatively low mole fraction of halon 1301 ($X_\infty = 0.025$) to extinguish methane flames, an increase in the flow velocity as a result of agent injection was neglected. However, because of substantial agent concentrations, particularly for nitrogen, the total (air and agent) effective mean velocity ($U_t^*$) was substituted into $U_a^*$ to calculate $\tau_{exp}$ (Fig. 3) and then $\tau_{eff}$ for all data in this paper. From Fig. 8, the coefficient $C$ was determined as 0.92, and thus,

$$\tau_{eff} = 0.92\tau_{exp} = 31.9(h_s/U_t^*) \tag{4}$$

$\tau_{eff}$ for each condition for the JP-8 flames is listed in Fig. 7.

Figure 8a indicates that the most data points scatter around the theoretical line within ±20% of $X_\infty$. Figure 8b shows the critical agent mole fraction at suppression normalized by the minimum value ($X_c/X_\infty$) vs. the agent injection period normalized by the effective mixing time in the recirculation zone ($\Delta t/\tau_{eff}$) with a theoretical curve (Eq. 2 with Eq. 4). The data points collapsed into a single curve independent of the agent and fuel types, the obstruction shape and height, and the mean inlet air velocity. The theoretical curve follows the data trend extremely well. It should be noted, however, that although Eq. 2 was originally derived based on the well-stirred reactor theory, it does not necessarily mean that the flame-flow phenomena in the recirculation zone resemble those in a well-stirred (premixed) reactor. OH PLIF observations rather revealed sheet-like wrinkled laminar diffusion flame zone at the interface of inhomogeneously stirred packets of the fuel and air. The theory worked well probably because the material exchange between the recirculation zone and free stream by the dynamic air entrainment might also be expressed, in a global sense, by the first-order differential equation (Eq. 1 in Takahashi et al., 2000).

The nondimensional representation of the results revealed that the critical agent mole fraction at suppression dramatically increased as the agent injection period decreased below the effective mixing time ($\Delta t/\tau_{eff} < 1$). Because the minimum agent mole fraction can be approximated by the value obtained by conventional steady-state methods (i.e., cup-burner flames or low-strain-rate counterflow diffusion flames) and the effective mixing time is correlated (Eq. 4)

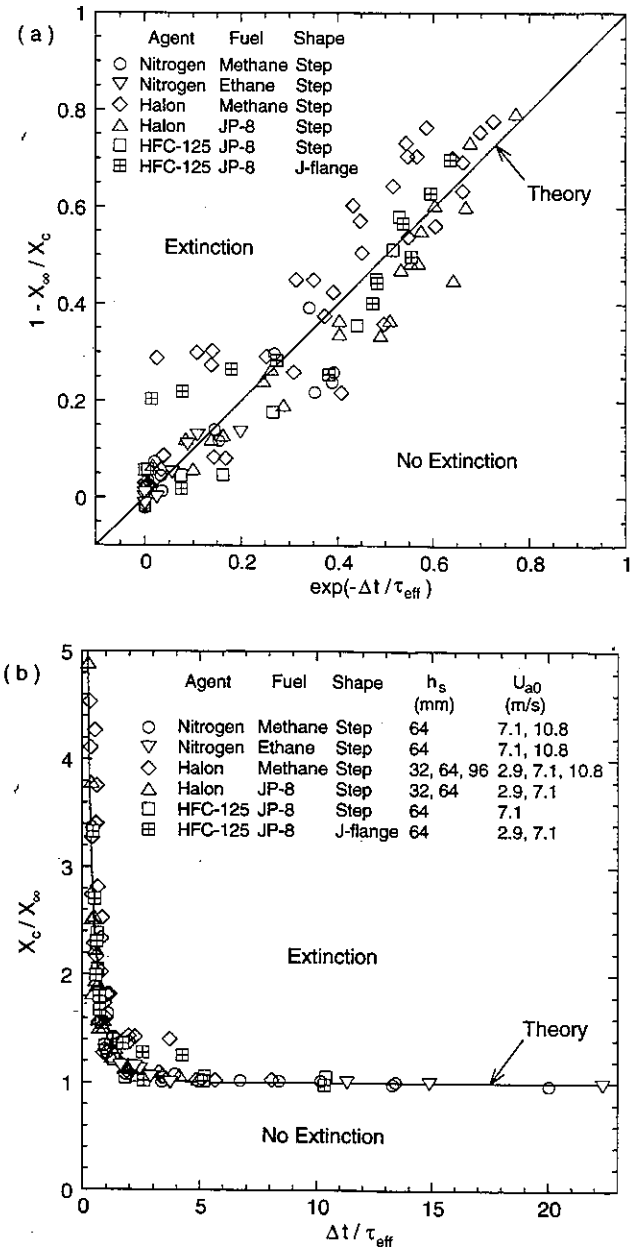


FIGURE 8 Nondimensional representations of the measured suppression limits and a theoretical curve for various agents, fuels, obstruction shapes, heights, and air velocities. (a) $(1 - X_\infty/X_c)$ vs. $\exp(-\Delta t/\tau_{eff})$; (b) $X_c/X_\infty$ vs. $\Delta t/\tau_{eff}$



to the experimental conditions (the step height and effective total mean air velocity), the suppression limit of step-stabilized flames can be predicted theoretically within an error bar of approximately ±20%.

## Suppression Mechanism

The extinction of diffusion flames is generally explained (Williams, 1974) by a critical Damköhler number ($Da = \tau_r/\tau_c$, $\tau_c$: the chemical time and $\tau_r$: the flow or diffusion time) below which extinction occurs. Thus, Da decreases either by decreasing $\tau_r$ or increasing $\tau_c$. Increasing the velocity gradient (strain rate) across the flame zone decreases $\tau_r$, thus leading to extinction by aerodynamic flame stretch. On the other hand, increasing the agent concentration decreases the flame temperature (thermal effects) and/or inhibits oxidation (chemical effects), thus increasing $\tau_c$, thus resulting in extinction by thermochemical effects. Nitrogen and HFC-125 are thermal suppressants, and halon 1301 is considered to be primarily chemical suppressant. In the present experiments, the air velocities were substantially smaller than those for blowout conditions with no agent and $X_\infty$ was independent of the airflow velocity as described earlier. Furthermore, the current results revealed that $X_\infty$ was similar to the values obtained by the steady-state cup-burner or low-strain-rate counterflow diffusion flame and that suppression occurred if the agent injection period was long enough to increase the agent mole fraction in the recirculation zone to $X_\infty$. In addition, even at high air velocities in regime II, freely moving (low strain rate) flame zones exist in the low-velocity recirculation zone in addition to the high-strain flame in the shear layer. Therefore, the suppression of obstruction-stabilized flames appears to occur by extinction of relatively low-strain-rate diffusion flames due to thermochemical causes. Although the experimental conditions of the data presented here are limited, the basic concept for suppression criterion obtained for a gaseous fuel using simple geometries must apply to liquid-fuel pool fires stabilized in more complex clutter configurations.

## CONCLUSIONS

The suppression limits of nonpremixed flames of methane, ethane, and JP-8, stabilized by a backward-facing step or J-flange in an airstream were measured as the critical agent mole fraction at suppression as a function of the unsteady injection period of a gaseous fire-extinguishing agent (nitrogen, halon 1301, or HFC-125) for various obstruction heights and air velocities. The steady-state

suppression limit was also measured by continuously adding nitrogen into the approach airflow in the ethane flame. The minimum agent mole fraction at suppression obtained at long injection periods in the transient method (0.292 and 0.365 for methane and ethane, respectively, with nitrogen; 0.04 and 0.087 for JP-8 with halon 1301 and HFC-125, respectively) or by the steady-state method (0.347 for ethane with nitrogen) did not vary much from the values obtained by the conventional steady-state methods, i.e., cup burners or laminar, relatively low strain-rate counterflow diffusion flames. Furthermore, OH PLIF images revealed the narrow, wrinkled laminar flame zone, which freely move with the fuel-air interface in response to the dynamic air entrainment. Therefore, the suppression process must be controlled by thermochemical extinction of the relatively low-strain-rate flames in the low-speed recirculation zone even at high free-stream velocities.

The obstruction-stabilized JP-8 pool fire may not be extinguished with halon 1301 at the conditions specified by the design criterion (6% agent concentration for 0.5-s duration) for the current fire-extinguishing system in the aircraft engine nacelle. The physical time is inappropriate to be used for the design criterion; instead, the effective mixing time, determined as $\tau_{\text{eff}} = 31.9[h_s/U_t^*]$, is more relevant to the extinction condition and should be considered in establishing a criterion. The measured extinction-limit data points collapsed into a single curve when plotting the critical agent mole fraction at extinction normalized by its minimum value obtained at long injection periods as a function of the agent injection period normalized by the effective mixing (residence) time. The data trend can be predicted by a theoretical expression using the minimum agent mole fraction and the effective mixing time. The effect of obstruction on the extinction limits is significant only when the agent injection period is less than the effective mixing time. These physical understanding and prediction capability would simplify testing of future agents and shift the practical design problem to one of quantifying the local velocity and obstruction size in the most likely location for a pool fire.

## Acknowledgements

This research is part of the Department of Defense's Next-Generation Fire Suppression Technology Program, funded by the DoD Strategic Environmental Research and Development Program, Sandia National Laboratories (SNL), Albuquerque, New Mexico, under Contract No. BF-3670, and the Air Force Research Laboratory, Propulsion Directorate, Propulsion Sciences and Advanced Concept Division, Wright-Patterson Air Force Base, Ohio, under Contract No. F33615–97-C-2719 (Technical Monitor: C. W. Frayne). The authors wish to acknowledge the assistance in conducting the PLIF experiment by Dr. Campbell D. Carter of Innovative Scientific Solutions, Inc., stimulating discussions with Dr. Sheldon R. Tieszen, Ms. Amalia R. Lopez, and Dr. Louis A. Gritzo of SNL, and valuable inputs for realistic test conditions and geometries by Mr. Mark Kay and Dr. Glen Harper of The Boeing Company.



## References

Babb, M., Gollahalli, S. R., and Sliepcevich, C. M. (1999). Extinguishment of liquid heptane and gaseous propane diffusion flames. *Journal of Propulsion and Power*, 15, 260–265.

Bajpai, S. N. (1974). An investigation of the extinction of diffusion flames by halons. *J. Fire and Flammability*, 5, 255.

Donbar, J. M., Driscoll, J. F., and Carter, C. D. (2000). Reaction zone structure in turbulent nonpremixed jet flames – from CH-OH PLIF Images. *Combustion and Flame*, 122, 1–19.

Dyer, J. H., Marjoram, M. J., and Simmons, R. F. (1977a). The extinction of fires in aircraft jet engines-Part III, Extinction of fires at low airflows. *Fire Technology*, 13, 126–138.

Dyer, J. H., Marjoram, M. J., and Simmons, R. F. (1977b). The extinction of fires in aircraft jet engines-Part IV, Extinction of fires by sprays of bromochlorodifluoromethane. *Fire Technology* 13, 223–230.

Gritzo, L. A., Tucker, J. R., Ash, L. (1999). Development of fire and suppression models for DoD vehicle compartments: background, objectives, and methodology. *Proceedings of the 9th Halon Options Technical Working Conference (HOTWC-99)*, Albuquerque, NM, pp. 34–44.

Grosshandler, W. L., Gann, R. G., and Pitts, W. M., Introduction (1994). Introduction. *Evaluation of Alternative In-Flight Fire Suppressants for Full-Scale Testing in Simulated Aircraft Engine Nacelles and Dry Bays (W. L. Grosshandler, R. G. Gann, and W. M. Pitts, Eds.)*, National Institute of Standards and Technology, NIST SP 861, pp. 1–12.

Hamins, A., Gmurczyk, G., Grosshandler, W., Rehwoldt, R. G., Vazquez, I., Cleary, T., Presser, C., and Seshadri, K. (1994a). Flame Suppression Effectiveness. *Evaluation of Alternative In-Flight Fire Suppressants for Full-Scale Testing in Simulated Aircraft Engine Nacelles and Dry Bays* (W. L. Grosshandler, R. G. Gann, and W. M. Pitts, Eds.), National Institute of Standards and Technology, NIST SP 861, pp. 345–465.

Hamins, A., Trees, D., Seshadri, K., and Chelliah, H. K. (1994b). Extinction of nonpremixed flames with halogenated fire suppressants. *Combustion and Flame*, 99, 221–230.

Hamins, A., Cleary, T., Borthwick, P., Gorchkov, N., McGrattan, K., Forney, G., Grosshandler, W., Presser, C., and Melton, L. (1995). Suppression of Engine Nacelle Fires. *Fire Suppression System Performance of Alternative Agents in Aircraft Engine and Dry Bay Laboratory Simulations* (R. G. Gann, Ed.), National Institute of Standards and Technology, NIST SP 890, Vol. II, pp. 1–199.

Hamins, A., Presser, C., and Melton, L. (1996). Suppression of a baffle-stabilized spray flame by halogenated agents. *Proceedings of The Combustion Institute*, 26, 1413–1420.

Hirst, R., and Booth, K., (1977). Measurements of flame-extinguishing concentrations. *Fire Technology*, 13, 4.

Hirst, R., Farenden, P. J., and Simmons, R. F. (1976). The extinction of fires in aircraft jet engines-Part I, Small-scale simulation of fires. *Fire Technology*, 12, 266–289.

Hirst, R., Farenden, P. J., and Simmons, R. F. (1977). The extinction of fires in aircraft jet engines-Part II, Full-scale fire tests. *Fire Technology*, 13, 59–67.

Hirst, R., and Sutton, D. (1961). The effect of reduced pressure and airflow on liquid surface diffusion flames. *Combustion and Flame*, 5, 319–330.

Longwell, J. P., Frost, E. E., and Weiss, M. A. (1953). Flame stability in bluff body recirculation zones. *Industrial and Engineering Chemistry*, 45, 1629–1633.

Moore, T. A., Weitz, C. A., and Tapscott, R. E. (1996). An update of NMERI cup-burner test results. *Proceedings of the 6th Halon Options Technical Working Conference (HOTWC-96)*,Albuquerque, NM, pp. 551–564.

Moussa, N. A. (1994). Effects of Clutter on Performance of Fire Suppression Agents in Aircraft Dry Bays and Engine Nacelles. Report prepared for Booz, Allen and Hamilton, Dayton, Ohio.

National Fire Protection Agency (1994). *Standard on Clean Agent Fire Extinguishing Systems*, NFPA 2001.

Papas, P., Fleming, J. W., and Sheinson, R. S. (1996). Extinction of non-premixed methane- and propane-air counterflow flames inhibited with $CF_4$, $CF_3H$ and $CF_3Br$. *Proceedings of The Combustion Institute*, 26, 1405–1411.

Pitts, W. M., and Blevins, L. G. (1999). An investigation of extinguishment by thermal agents using detailed chemical modeling of opposed-flow diffusion flames. *Proceedings of the 9th Halon Options Technical Working Conference (HOTWC-99)*, Albuquerque, NM, pp. 145–156.

Raghunandan, B. N., and Yogesh, G. P. (1989). Recirculating flow over a burning surface-flame structure and heat transfer augmentation. *Proceedings of The Combustion Institute*, 22, 1501–1507.

Rohmat, T. A., Katoh, H., Obara, T., Yoshihashi, T., and Ohyagi, S. (1998). Diffusion flame stabilized on a porous plate in a parallel airstream. *AIAA J.* 36, 1945–1952.

Saito, N., Ogawa, Y., Saso, Y., and Sakai, R. (1996). Improvement on Reproducibility of Flame Extinguishing Concentration Measured by Cup Burner Method. Report of Fire Research Institute of Japan, No. 81, pp. 22–29.

Sakai, R., Saito, N., Saso, Y., Ogawa, Y., and Inoue, Y. (1995). Flame Extinguishing Concentrations of Halon Replacements for Flammable Liquids. Report of Fire Research Institute of Japan, No. 80, pp. 36–42.

Saso, Y., Saito, N., Liao, C., and Ogawa, Y. (1996). Extinction of counterflow diffusion flames with halon replacements. *Fire Safety Journal*, 26, 303–326.

Sheinson, R. S., Pener-Hahn, J. E., and Indritz, D. (1989). The physical and chemical action of fire suppressants. *Fire Safety Journal*, 15, 437–450.

Simmons, R. F., and Wolfhard, H. G. (1957). Some limiting oxygen concentrations for diffusion flames in air diluted with nitrogen. *Combustion and Flame*, 1, 155–161.

Takahashi, F., Schmoll, W. J., Strader, E. A., and Belovich, V. M. (2000). Suppression of a non-premixed flame stabilized by a backward-facing step. *Combustion and Flame*, 122, 105–116.

Tieszen, S. R., and Lopez, A. R. (1999). Issues in numerical simulation of fire suppression. *Proceedings of the 9th Halon Options Technical Working Conference (HOTWC-99)*, Albuquerque, NM, pp. 178–190.

Tsuji, H. (1982). Counter flow diffusion flames. *Prog. Energy Combust. Sci.*, 8, 93–119.

United Nations Environment Programme (UNEP) (1994). *Report of the Halon Fire Extinguishing Agents Technical Options Committee.*

Williams, F. A. (1974). A unified view of fire suppression. *Journal of Fire & Flammability*, 5, 54–63.

Winterfeld, G. (1965). On processes of turbulent exchange behind flame holders. *Proceedings of The Combustion Institute*, 10, 1265–1275.